Performance Characterization of Ultrahigh Speed Optically Amplified Spectral-Phase Encoded OCDMA Systems with Second-Harmonic-Generation Effect in *Thin* and *Thick* Crystal Receiver Structures

Mehdi D. Matinfar, *Student Member, IEEE*, and Jawad A. Salehi, *Fellow, IEEE*

***Abstract*—In this paper we study and evaluate the performance of a spectral-phase encoded optical CDMA (SPE-OCDMA) system using advanced receiver structures based on second harmonic generation (SHG) effect imposed in a *Thick* or *Thin* crystal. This receiver structure is employed as the nonlinear pre-processor prior to the conventional low-speed photodetector. In our performance evaluation amplified spontaneous emission (ASE) of the optical amplifiers, receiver front end thermal noise and photodetector shot noise which are effective in low power conditions, and multiple access interference (MAI) noise which is the dominant source of noise in high power conditions in any coherent OCDMA communications system have been considered. We begin by studying the statistical behavior of *Thick* crystals in an optically amplified digital lightwave communication system in the context of a SPE-OCDMA communication system. The error probability for *Thick* crystal receiver structure is evaluated using Saddle-Point approximation. Furthermore, we obtain a closed form approximation for the probability density function (pdf) of the decision variable in SPE-OCDMA systems with *Thin* crystal SHG receiver. In this analysis, to obtain approximate probability density function, we employ Gram-Charlier expansion based on the corresponding first order moments of the decision variable. The first three moments are obtained in a closed form approximation and consequently a closed form expression for the error probability is obtained by integrating the approximated pdf of the decision variables for transmitting bit "1" and "0" in *Thin* crystal receiver structure. The precision of the approximation is verified by the Monte-Carlo simulation. Finally the performance of SPE-OCDMA network for both *Thin* and *Thick* SHG crystals are analytically evaluated and discussed for different number of interfering users and different code-lengths and different speed of the conventional photodetectors. We deduce that the performance of *Thin* SHG crystal receiver is more sensitive to the transmitted power level especially in low power conditions. It is concluded that in low power conditions where ASE, thermal and shot noises are the dominant noise sources, *Thick* SHG crystal receiver outperforms the *Thin* crystal receiver. However, in high power conditions where MAI noise is the most effective noise term, *Thin* SHG crystal receiver structure outperforms the *Thick* crystal receiver.**

Paper approved by K. Kitayama, the Editor for Photonic Networks and Fiber Optic Wireless of the IEEE Communications Society. Manuscript received September 29, 2009; revised November 2, 2010.

This work was supported in part by the Iran National Science Foundation (INSF).

The authors are with the Optical Networks Research Laboratory (ONRL), Electrical Engineering Department, Sharif University of Technology, Tehran, Iran (e-mail: m.d.matinfar@gmail.com; jasalehi@sharif.edu).

Digital Object Identifier 10.1109/TCOMM.2011.062311.090573

***Index Terms*—Spectral phase encoded OCDMA, second harmonic generation (SHG), Gram-Charlier expansion, lightwave communication systems, ultra-short light pulse, ultrahigh speed detection scheme, optical *thin* and *thick* crystals.**

I. Introduction

AMONG various optical code division multiple access (OCDMA) systems spectrally-phase-encoded OCDMA (SPE-OCDMA), due to its powerful means of encoding/decoding, is the most promising OCDMA system for many upcoming all-optical networking [1]. One of the most challenging aspects of such systems is related to its ability in identifying the presence of ultrashort light pulses, e.g., femto-sec, subpico-sec, in the presence of multiple access interference (MAI). For such detection scheme we require to either use ultra-fast sampling technology on the order of pico and femto-second for optimum detection or to use a powerful alternative, but sub-optimum, namely all-optical non-linear detection such as second-harmonic-generation (SHG), two-photon-absorption (TPA), or highly nonlinear fiber (HNLF) [2-4]. In general a conventional photodetector used for detection of correctly decoded ultrashort light pulse can simply be modeled as an energy detector which evaluates the pulse energy in its response time. In order to obtain the best detection performance, the photodetectors must have a response time equal to the pulse width. However, practical photodetectors have a response time on the order of 9 pico-sec that is much more than the typical pulse width used in SPE-OCDMA which are on the order of subpico-sec [9]. The response time of conventional photodetectors is typically on the order of 100 to 1000 times the pulse width which it is on the order of spreading duration of the encoded or incorrectly decoded pulses in SPE-OCDMA systems. Since the energies of incorrectly decoded pulses are within the same order of the properly decoded pulse, the performance of such systems surely degrades if there is no pre-processing device prior to the low speed photodetector [11]. Most enabling technologies proposed for implementing the pre-processors are based on imposing a nonlinear effect in a photonic waveguide with a large amount of discrimination between the high and low peak power signal. Two Photon Absorption (TPA) detectors

where their output is proportional to the square of the input light intensity is one of those enabling technologies where the pre-processor and the photodetector parts are integrated in a single device. Self Phase Modulation (SPM) effect which is imposed in special fibers with high nonlinearity coefficient namely Highly Non-Linear Fiber (HNLF) and Second Harmonic Generation effect which is imposed in some types of dielectric crystals are other enabling technologies employed as pre-processors prior to conventional low speed photodetectors. The feasibilities and applicabilities of these methods are shown in SPE-OCDMA system in many experimental studies [2-6]. However; the analytical approaches to study the statistical behavior of such sub-optimum schemes have received less attention due to its mathematical complexity. Recently in [7] the performance of a RZ-OOK lightwave communication system using a TPA detector as the nonlinear receiver was evaluated and reported. The resulting model was employed in a SPE-OCDMA system and the performance of such a system was obtained and discussed in [8]. In [9] performance of a SPE-OCDMA system using SPM and SHG nonlinear pre-processor was obtained. Due to its mathematical complexity, the authors succeeded in evaluating the performance of the system using Monte-Carlo simulation. In [10], an approach was proposed to investigate the effect of the combination of highly nonlinear fiber and optical band pass filter as the preprocessor prior to the photodetector. In this approach, the amount of spreading in frequency spectrum is defined as the decision variable and the authors obtain the mean and the variance of the decision variable, and the probability of error is obtained using Gaussian approximation. However, in this paper second harmonic generation (SHG) effect in *Thick* crystal which was studied in an ultrahigh speed lightwave communication receiver [11], is considered in a SPE-OCDMA system. In evaluating the performance of such systems we begin by obtaining the moment generating function (MGF) of the decision variables at the output of the sampler after the *Thick* SHG crystal. Using the output MGF of the decision variables in Saddle-Point approximation method we can evaluate the performance of the system for different parameters of the network such as the number of users and the user's code length with high precision. Also in this paper we present and study an analytical approach using the Gram-Charlier expansion in modeling the statistical behavior of *Thin* SHG crystals. Finally, the closed form approximation for the total error probability of SPE-OCDMA system with *Thick* crystal receiver structure is obtained. The results of this study are used in a SPE-OCDMA communication system in order to present its performance using various system parameters. The rest of this paper is organized as follows. In Section II the concept of spectral phase encoding-decoding technique and the detailed description of different building blocks of a SPE-OCDMA using SHG receiver structure are presented. In Section III the Second Harmonic Generation effect, the dominant nonlinear effect in some dielectric crystals, is introduced and the mathematical models for two extreme behaviors of this device namely *Thin* and *Thick* crystals in the context of digital lightwave communication systems are described. In Section IV the statistical model of the SHG effect used as a pre-processor in ultra-high speed optical communication systems for two separate regimes, i.e., *Thin* and *Thick*, is presented. This model is used for the performance evaluation of a SPE-OCDMA receiver with SHG crystals as the pre-processor prior to the photodetectors. The impact of thermal noise due to the front end electronic circuitry and shot noise corresponding to the photodetector is studied in Section V. In Section VI the numerical results are presented and an in-depth discussion on the performance of the SPE-OCDMA for various parameters is presented. Finally, Section VII concludes the paper.

II. SPE-OCDMA System Description With SHG Receiver Structure

A typical SPE-OCDMA network with *N* users is shown in Fig. 1. In such a system each user transmits its information bit using OOK signaling scheme in which for transmitting bit "1" a band-limited ultrashort light pulse, $A(t)$ with duration T_c, e.g., on the order of $100fs$, is transmitted within one bit duration T_b and for transmitting bit "0" no pulse is transmitted. At the transmitter side, the frequency spectrum of the band-limited pulse with bandwidth *W* is divided into N_0 frequency chips or bins such that $W \triangleq N_0\Delta\omega$ where, $\Delta\omega$ is the bandwidth of each of the frequency bins. A family of *N* pseudo-random binary signature sequences $\{C_j\}_{j=1}^{N}$, each assigned to a particular user, plays a key role in a SPE-OCDMA network. In this paper we assume all pseudo-random binary codes have equal length N_0 with components that are randomly selected from the binary set $\left\{e^{j0}=1, e^{j\pi}=-1\right\}$ with equal probability. The encoder due to *j*th user adds 0 or π values to the phases of the frequency bins corresponding to the *j*th user according to the elements of the assigned code C_j. In [12], it is shown that when random coding is used as the signature sequence for each user, the encoder spreads the incident pulse in time by a factor of N_0 and a noise-like low intensity signal with duration $T = N_0T_c$ is formed at the encoder output with T_c being the assigned pulse duration. It should be noted that the spreading time T is not necessarily equal to the bit interval . In fact, the ratio between the bit interval T_b and the spreading time *T* is called the excess spreading factor which is denoted by *K*. It is usually assumed that the excess spreading factor $K \triangleq T_b/T$ is an integer number. Finally the encoder's output enters into the fiber optic channel, shared among all of the network users through the star coupler, and is interfered with other users encoded signal. The signal due to *j*th user is added to the multiple access interference (MAI) signal and the result arrives at the receiver input of the *j*th user. After amplification and filtering with an optical amplifier and an optical band-pass filter a band-limited white random process, due to the amplified spontaneous emission (ASE) noise of the optical amplifier, is added further to the received signal. L_1 and L_2 are total fiber losses before and after the optical amplifier. G_{amp} denotes the gain of optical amplifier. By assuming an ideal star-coupler with *N* branches, the total amplification and losses along the path is obtained as $G = \frac{G_{amp}L_1L_2}{N}$ [22]. The resulting signal enters the *j*th decoder which is similar to the *j*th encoder apart from the used signature sequence which is the complex conjugate of the corresponding sequence used in the corresponding encoder. When the input to the *j*th

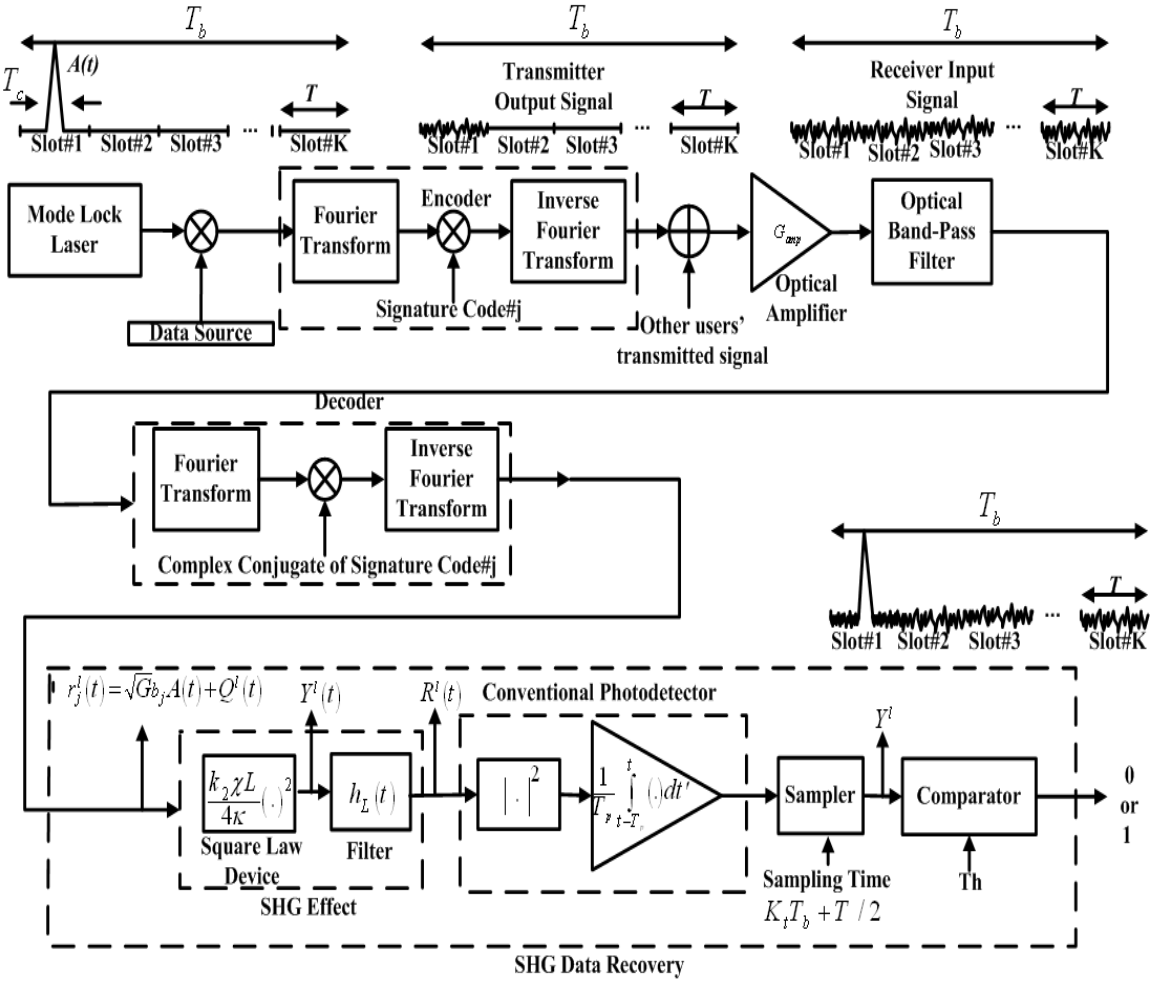

Fig. 1. A typical spectral-phase encoded OCDMA system employing the optical SHG crystal as the data recovery subsystem.

decoder is the pulse coded with signature sequence C_j the output is recovered as the original short pulse with duration T_c otherwise, due to the random properties of the code elements, the output remains in the form of a low intensity noise-like signal [12]. So, the *j*th decoder output is the summation of a band-limited noise due to MAI and ASE and a short pulse when data bit "1" is transmitted, otherwise, it only consists of a band-limited noise term. Finally, the decoder output enters the data recovery sub-system which in this paper it consists of a second harmonic generation crystal as the pre-processor prior to a conventional photodetector. In subsequent sections after presenting an introduction to the mathematical modeling of the nonlinear SHG effect the error probability of the aforementioned system is obtained.

III. Mathematical Modeling of Second Harmonic Generation Effect

In this section a simple mathematical model for a nonlinear second harmonic generation (SHG) effect in photonic crystals is presented. In such dielectric crystals when satisfying phase matching conditions between the fundamental and second harmonic waves a nonlinear effect namely second harmonic generation dominates among other nonlinear effects. In the most simple case, the perfect phase matching between the fundamental and second harmonic waves happens when the wave number due to the second harmonic wave becomes twice the corresponding wave number of the fundamental wave [14]. When a high power optical wave at frequency ω_0 enters the crystal in which the phases of the fundamental and second harmonic waves are matched then certain amount of energy efficiently transfers to the second harmonic wave at frequency $2\omega_0$. These phase matching conditions are hardly satisfied in the case that the input wave is an ultrashort light pulse, mainly due to its wide-band frequency content. In [14] by relaxing some phase matching conditions, the transient behavior of the photonic crystals in response to the wide-pulses has been studied when the SHG effect dominates among the other higher order nonlinearities. Hereafter, in this paper, crystals with dominant SHG effect are called SHG crystals. These crystals are classified into two general forms namely *Thin* and *Thick* SHG crystals. This classification is obtained according to the length of the crystals. For the aforementioned classification, a parameter namely walk-off length, denoted by L_w, is defined as follows,

$$L_w \triangleq \frac{T_c}{GVM} \tag{1}$$

Where $GVM \triangleq |1/V_{g_1} - 1/V_{g_2}|$ is defined as the group velocity mismatch (GVM) between the fundamental and second

harmonic waves in the SHG crystal. In general, if the crystal length is much greater than the walk-off length, i.e., $L \gg L_w$, the crystal is assumed to be in *Thick* regime, which it can be safely modeled as the cascade of a nonlinear square-law device with a linear low-pass filter with a bandwidth inversely proportional to the crystal length as follows [11],

$$E_{out}(t) = h_L(t) * \left[C \times E_{in}^2(t)\right] \tag{2}$$

Where $h_L(t)$ in the above equation denotes the impulse response of the low-pass filter in the *Thick* crystal model which is defined as follows,

$$h_L(t) = \begin{cases} \frac{1}{L\left(1/V_{g_2} - 1/V_{g_1}\right)} & L/V_{g_1} < t < L/V_{g_2} \\ 0 & Otherwise \end{cases} \tag{3}$$

On the other hand, if the crystal length is much less than the walk-off length, i.e., $L \ll L_w$, then it is classified as a *Thin* crystal and is simply modeled as a nonlinear square-law device and its input/output relation is expressed as follows [11],

$$E_{out}(t) = C \times E_{in}^2(t) \tag{4}$$

In equations (2) and (4), $E_{in}(t)$ and $E_{out}(t)$ are the envelope of the input and output fields of the SHG crystal, respectively. It should be noted that in both, *Thick* and *Thin* crystals, the carrier frequency of the output field $E_2(t)$ is twice the carrier frequency of the input field. The parameter C in equations (2) and (4) is the conversion coefficient of the crystal which is defined as $C \triangleq L \times P_c$. Where P_c indicates the physical parameter of the crystal and it is defined as $P_c = \frac{k_2 \chi}{4\kappa}$ with the parameters κ and χ representing the dielectric constant and the second order susceptibility of the crystal and k_2 denotes the second harmonic wave number.

IV. Performance Characterization of SPE-OCDMA With SHG Pre-processor

In this section we obtain the error probability corresponding to the *j*th user's *(j=1,2,,,N)* receiver. Let $E_k(t)$ denote the received field corresponding to the *k*th user and $E_{kj}(t)$ is the *j*th decoder output when $E_k(t)$ is its input. For the sake of simplicity in presentation, hereafter, we assume that there exist l active interfering users, i.e., l interfering users transmit bit "1," and the corresponding detection error probability is denoted by PE_l. Therefore, the total error probability will be computed by averaging the error probabilities $\{PE_l\}_{l=0}^{N-1}$ over the number of interfering users l [12]. The *j*th decoder output $r_j^l(t)$ given l active interfering users can be represented as follows,

$$r_j^l(t) = \sqrt{G} E_{jj}(t) + \sqrt{G} \sum_{k \neq j, k \in B_a} E_{kj}(t) + Z_{ASE}(t) \tag{5}$$

The set B_a, with l integers as its elements chosen from the set $\{1, 2, ..., N\}$, contains the active interfering user's indices. In the above equation, *G* is the total amplification and losses of the path as defined before and $Z_{ASE}(t) = p(t) + jq(t)$ is the base-band equivalent of the filtered optical amplifier noise which is assumed to be a band-limited white process with $p(t)$ and $q(t)$ as its quadrature components [13]. The random process $Z_{ASE}(t)$ has a two sided spectral density equal to $\delta/2$, with $\delta \triangleq n_{sp}(G_{amp} - 1) h\upsilon$[13], where n_{sp} is the spontaneous emission parameter, h is the Planck constant and $\upsilon = \omega_0/(2\pi)$ is the frequency of the incident optical signal. If we define $Z_{l,interference}(t) \triangleq \sqrt{G} \sum_{k \neq j, k \in B_a} E_{kj}(t)$ as the summation of l Gaussian random processes then $Z_{l,interference}(t)$ remains also as a Gaussian random process. The decoded signal $E_{jj}(t)$ consists of an ultrashort light pulse when *j*th user transmits bit "1," otherwise, it equals to zero. Therefore, $r_j^l(t)$ is the summation of a Gaussian band-limited white process and a short pulse when bit "1" is transmitted, otherwise it is a Gaussian band-limited random process due to the summation of MAI and ASE noises. Due to the limiting speed of conventional photodetectors, it is becoming a common practice to place an optical nonlinear element prior to the photodetector in order to avoid severe performance degradation [11]. In this paper we employ both *Thin* and *Thick* second harmonic generation (SHG) crystals as the nonlinear pre-processor prior to a conventional and low speed photodetector. From (5) the decoded signal which is the input to the SHG crystal for the *j*th user can be represented as follows,

$$r_j^l(t) = \sqrt{G} b_j A(t) + Q^l(t) \qquad -T_b/2 \leq t < T_b/2 \tag{6}$$

Where, b_j is the transmitted bit due to the desired user, i.e., *j*th user, which can be 1 or 0, $A(t)$ is the reconstructed or the original ultrashort light pulse and, for the sake of mathematical simplicity in obtaining a closed form error probability expression, it is assumed to be a rectangular pulse with a pulse width equal to T_c and an amplitude equal to $\sqrt{G \times P_t}$ where P_t denotes the peak power of the transmitted pulse. In the above equation, $Q^l(t)$ is the accumulated sum of optical amplifier ASE noise and the MAI noise due to l active interfering users, denoted by $Z_{l,interference}(t)$. Both of $Z_{ASE}(t)$ and $Z_{l,interference}(t)$ can be assumed to be Gaussian [12], [13]. So, we have,

$$Q^l(t) = Z_{l,interference}(t) + Z_{ASE}(t) \tag{7}$$

$Z_{l,interference}(t)$ and $Z_{ASE}(t)$ are modeled as a zero mean band-limited Gaussian random process with autocorrelation functions $R_{l,interference}(\tau) = \sigma_{l,interference}^2 Sinc(\tau/T_c)$ and $R_{ASE}(\tau) = \sigma_{ASE}^2 Sinc(\tau/T_c)$ respectively. $\sigma_{l,interference}^2$ and σ_{ASE}^2 are the corresponding MAI and ASE noise variances which can be expressed as follows,

$$\begin{aligned} \sigma_{l,\text{interference}}^2 &= \tfrac{lGP_t}{N_0} \\ \sigma_{ASE}^2 &= \tfrac{\delta}{T_c} \end{aligned} \tag{8}$$

The optical band pass filter at the receiver input is assumed to have the minimum required bandwidth ($B_o = \frac{1}{T_c}$) in order to keep the maximum pulse energy and reject the excessive noise energy [21]. In this paper, for the sake of mathematical simplicity, in obtaining the closed form expressions for the error probabilities $\{PE_l\}_{l=0}^{N-1}$, the sinc-shape autocorrelation functions are approximated by a triangular pulse with the same amplitude. Because of the statistical independence between ASE noise $Z_{ASE}(t)$ and MAI noise $Z_{l,interference}(t)$, the equivalent variance due to the noise $Q^l(t)$ is obtained as $\sigma_l^2 = \sigma_{ASE}^2 + \sigma_{l,interference}^2$. In this stage, all the conditional error probabilities $\{PE_l\}_{l=0}^{N-1}$, given l interfering users, are

evaluated without including the thermal noise due to the electronic circuitry, and the shot noise and the dark current noise due to the photodetector. However, Section V is dedicated to investigate the impact of the above aforementioned noise sources along with the MAI and ASE. Based upon equation (6) and due to Gaussian statistics of $Q^l(t)$, the probability PE_l is inferred as the error probability of the SHG data recovery sub-system in detecting the presence of the light pulse $A(t)$ in an additive Gaussian noise environment. It should be noted that this problem has been studied, analytically, in [11] for *Thick* SHG crystal pre-processor. So, the error probabilities $\{PE_l\}_{l=0}^{N-1}$ in *Thick* crystal case, can be computed by applying the same approach presented in [11].

A. Derivation of PE_l for Thick SHG Crystal Pre-processor

Based on the mathematical model presented in Section III for *Thick* SHG crystal and by substituting $r_j^l(t)$ for $E_{in}(t)$ in equation (2), the SHG crystal output $R^l(t)$ is obtained as $R^l(t) = h_L(t) * Y^l(t)$ where $Y^l(t)$ denotes the square-law device output in the represented model. Let Y^l denote the decision variable in SHG data recovery sub-system for l active interfering users then we have [11],

$$Y^l = \frac{1}{T_p}\int_{-T_p/2}^{T_p/2} \left|R^l(t)\right|^2 dt = T_p^2 \sum_{n=-m_l}^{m_l} \left|y_n^l H_L(n)\right|^2 \quad (9)$$

Where $\{H_L(n)\}_{n=-\infty}^{+\infty}$ denotes the Fourier coefficients due to the impulse response $h_L(t)$ and T_p indicates the photodetector integration time. The low-pass filter in *Thick* SHG crystal model is Sinc-shape in frequency domain which can be, approximately, assumed band-limited in its main lobe. In the above equation, $\{y_n^l\}_{n=-m_l}^{m_l}$ are the Fourier coefficients due to $Y^l(t)$ falling into the SHG filter window, i.e.,$[-m_l, ..., m_l]$, where m_l is the cut-off index of the Fourier coefficients corresponding to the low-pass filter $h_L(t)$ in SHG crystal model. It can be easily deduced from (3) that if $T_L = L \times GVM$ is the time duration of the impulse response $h_L(t)$ then m_l is obtained as $m_l = \lfloor T_p/T_L \rfloor$. Based upon Papoulis's well known theorem on Gaussianity on narrow-band systems output and by applying the conditions corresponding to *Thick* SHG crystal it can be deduced that the Fourier coefficients $\{y_n^l\}_{n=-m_l}^{m_l}$ are jointly Gaussian random variables [15]. In order to evaluate the error probability PE_l the random vectors $\vec{V}_1^l$ and $\vec{V}_0^l$ are defined as follows,

$$\begin{aligned}
\left(\vec{V}_1^r\right)^T &\triangleq Real\left\{\begin{bmatrix} y_{-m_l}^l, y_{-m_l+1}^l, y_{-m_l+2}^l, ..., \\ y_0, ..., y_{m_l-1}^l, y_{m_l}^l \end{bmatrix} |1\right\} \\
\left(\vec{V}_1^i\right)^T &\triangleq \mathrm{Im}ag\left\{\begin{bmatrix} y_{-m_l}^l, y_{-m_l+1}^l, y_{-m_l+2}^l, ..., \\ y_0, ..., y_{m_l-1}^l, y_{m_l}^l \end{bmatrix} |1\right\} \\
\left(\vec{V}_1^l\right)^T &\triangleq \left[\left(\vec{V}_1^r\right)^T, \left(\vec{V}_1^i\right)^T\right] \\
\left(\vec{V}_0^r\right)^T &\triangleq Real\left\{\begin{bmatrix} y_{-m_l}^l, y_{-m_l+1}^l, y_{-m_l+2}^l, ..., \\ y_0, ..., y_{m_l-1}^l, y_{m_l}^l \end{bmatrix} |0\right\} \\
\left(\vec{V}_0^i\right)^T &\triangleq \mathrm{Im}ag\left\{\begin{bmatrix} y_{-m_l}^l, y_{-m_l+1}^l, y_{-m_l+2}^l, ..., \\ y_0, ..., y_{m_l-1}^l, y_{m_l}^l \end{bmatrix} |0\right\} \\
\left(\vec{V}_0^l\right)^T &\triangleq \left[\left(\vec{V}_0^r\right)^T, \left(\vec{V}_0^i\right)^T\right]
\end{aligned} \quad (10)$$

Using equation (9) the decision variables Y_0^l and Y_1^l for transmitting bit "0" and bit "1" are obtained as follows,

$$\begin{aligned}
Y_0^l &= \left(\vec{V}_0^l\right)^T Q_{2(2m_l+1)} \left(\vec{V}_0^l\right) \\
Y_1^l &= \left(\vec{V}_1^l\right)^T Q_{2(2m_l+1)} \left(\vec{V}_1^l\right)
\end{aligned} \quad (11)$$

Where $Q_{2(2m_l+1)}$ is a diagonal matrix with the order $2(2m_l+1)$ and where its main diagonal elements denoted by $\{q_{n,n}\}_{n=1}^{2(2m_l+1)}$ are proportional to the Fourier coefficients of the low-pass filter $h_L(t)$,

$$\begin{aligned}
q_{n,n} = q_{n+2m_l+1,n+2m_l+1} &= T_p^2 \left|H_L(n-m_l-1)\right|^2 \\
&= Sinc^2\left(\tfrac{n-m_l-1}{m_l}\right) \qquad n = 1, 2, 3, ..., 2m_l+1
\end{aligned} \quad (12)$$

Let us denote $\Psi_0^l(s)$ and $\Psi_1^l(s)$ as the characteristic functions of the decision variable Y^l for transmitting bit "0" and "1" respectively. With the aid of Turin lemma [16] in evaluating the characteristic function of the quadratic forms of Gaussian random variables the corresponding characteristic functions of Y_1^l and Y_0^l denoted by $\Psi_1^l(s)$ and $\Psi_0^l(s)$ are obtained as follows [11],

$$\begin{aligned}
\Psi_1^l(s) &= \frac{1}{\left[\det\left(I_{2(2m_l+1)} - 2s\Phi_1^l Q_{2(2m_l+1)}\right)\right]^{1/2}} \\
&\quad \times \exp\left\{ \begin{array}{l} -(1/2)\left(\vec{\eta}_1\right)^T \left(\Phi_1^l\right)^{-1} \\ \left[\begin{array}{l} I_{2(2m_l+1)} - \\ \left(I_{2(2m_l+1)} - 2s\Phi_1^l Q_{2(2m_l+1)}\right)^{-1} \end{array}\right] \vec{\eta}_1 \end{array} \right\} \\
\Psi_0^l(s) &= \frac{1}{\left[\det\left(I_{2(2m_l+1)} - 2s\Phi_0^l Q_{2(2m_l+1)}\right)\right]^{1/2}}
\end{aligned} \quad (13)$$

In the above equation, Φ_1^l and Φ_0^l are the covariance matrices and $\vec{\eta}_1$ and $\vec{\eta}_0$ are the mean vectors corresponding to the vectors $\vec{V}_1^l$ and $\vec{V}_1^0$ respectively and $I_{2(2m_l+1)}$ represents the identity matrix of order $2(2m_l+1)$. The elements of Φ_1^l, Φ_0^l, $\vec{\eta}_1$, and $\vec{\eta}_0$ are evaluated similar to the approach in [11]. Finally, the conditional error probability PE_l for l interfering users is evaluated using the Saddle-Point approximation method [17].

B. Derivation of PE_l for Thin SHG Crystal Pre-processor

The decision variable which is obtained for *Thin* SHG data recovery sub-system corresponding to the *j*th user with l active interfering users can be expressed as follows [11],

$$Y^l = \frac{C^2}{T_p}\int_{-T_p/2}^{T_p/2} \left|r_j^l(t)\right|^4 dt \quad (14)$$

In (14) T_p denotes the integration time of the photodetector and $r_j^l(t) = \sqrt{G} b_j A(t) + Q^l(t)$, defined in equation (6), represents the input signal of SHG data recovery sub-system shown in Fig. 1. To evaluate the error probability PE_l we need to estimate the probability density function (pdf) of the decision variable Y^l. Note that, the decision variable is not Gaussian at the sampler output for *Thin* and *Thick* SHG crystals [11]. So, it is necessary to evaluate the pdf of the decision variable for accurate performance characterization. We employ a well-known Gram-Charlier function expansion for approximating the pdf of the decision variable since one can obtain

its statistical moments using analytical approach. Gaussian function as the Gram-Charlier kernel results in not such a good approximation in approximating the corresponding pdf of the decision variable Y^l, so we have chosen the Gamma kernel which is preferable for positive random variables. Using Gram-Charlier expansion with Gamma function as its kernel the pdf of the decision variable Y^l is approximated with four terms of the expansion as follows [18],

$$\begin{array}{l} f^l(x) = g\left(x/\beta_l\right) \approx e^{-(x/\beta_l)}\left(x/\beta_l\right)^{\alpha_l} \\ \left[\begin{array}{l} c_0^l L_0^{\alpha_l}\left(x/\beta_l\right) + c_1^l L_1^{\alpha_l}\left(x/\beta_l\right) \\ +c_2^l L_2^{\alpha_l}\left(x/\beta_l\right) + c_3^l L_3^{\alpha_l}\left(x/\beta_l\right) \end{array}\right] \end{array} \tag{15}$$

Where $L_0^{\alpha_l}(x)$,$L_1^{\alpha_l}(x)$, $L_2^{\alpha_l}(x)$ and $L_3^{\alpha_l}(x)$ in the above equation are the Laguerre polynomials of the first, second, third and fourth degree with the parameter α_l. The function $\varphi^{\alpha_l}(x) = e^{-x}x^{\alpha_l}$ is the Gamma function which is considered as the kernel of the Gram-Charlier expansion and c_0^l,c_1^l ,c_2^l and c_3^l are the expansion coefficients. With selecting appropriate values for α_l and β_l the first and second coefficients c_1^l and c_2^l can be assumed to be 0. So we have [18],

$$\begin{array}{l} f^l(x) = g\left(x/\beta_l\right) \approx e^{-(x/\beta_l)}\left(x/\beta_l\right)^{\alpha_l} \\ \left[c_0^l L_0^{\alpha_l}\left(x/\beta_l\right) + c_3^l L_3^{\alpha_l}\left(x/\beta_l\right)\right] \end{array} \tag{16}$$

With the above assumption the coefficients c_0^l and c_3^l are computed in Appendix (A) as follows [18],

$$\begin{array}{l} c_0^l = \frac{1}{\beta_l \Gamma(\alpha_l+1)} \\ c_3^l = \frac{1}{\beta_l \Gamma(\alpha_l+4)}\left[\frac{m_2^l}{\beta_l^2}\left(\alpha_l+3\right) - \frac{m_3^l}{\beta_l^3}\right] \end{array} \tag{17}$$

The suitable values for α_l and β_l that lead us to the above form of Gram-Charlier expansion are evaluated in Appendix (A) as follows,

$$\alpha_l = \frac{\left(m_1^l\right)^2}{m_2^l - \left(m_1^l\right)^2} - 1 \quad , \quad \beta_l = \frac{m_2^l - \left(m_1^l\right)^2}{m_1^l} \tag{18}$$

In the above equation, m_1^l, m_2^l and m_3^l are the first, second and third order moments of the decision variable Y^l respectively. These moments are obtained in closed form expressions in Appendices (B) and (C) for transmitting bit "0" and "1." The probability density functions for transmitting bit "1" and "0" are denoted by $f_1^l(x)$ and $f_0^l(x)$, respectively. The error probabilities for transmitting bit "1" and "0" denoted by PE_1^l and PE_0^l are computed as follows,

$$\begin{array}{l} PE_1^l = \int_{-\infty}^{Th} f_1^l(x)\,dx \quad , \quad PE_0^l = 1 - \int_{-\infty}^{Th} f_0^l(x)\,dx \\ PE_l = \frac{1}{2}\left(PE_1^l + PE_2^l\right) \end{array} \tag{19}$$

In the above equation *Th* indicates the optimum threshold for the comparator used in SHG data recovery sub-system in order to make a decision with minimum total error probability. According to the above equation, by integrating the pdf computed in (16) for transmitting bit "1" i.e., $f_1^l(x)$, the closed form expression for evaluating PE_1^l is obtained as follows,

$$\begin{array}{l} PE_1^l = c_0^l \beta_l \Gamma\left(\alpha_l+1\right)\gamma_{\alpha_l+1}\left(\frac{Th}{\beta_l}\right) + \\ \frac{c_3^l}{6}\left(\alpha_l+1\right)\left(\alpha_l+2\right)\left(\alpha_l+3\right)\beta_l\Gamma\left(\alpha_l+1\right)\gamma_{\alpha_l+1}\left(\frac{Th}{\beta_l}\right) - \\ \frac{c_3^l}{2}\left(\alpha_l+2\right)\left(\alpha_l+3\right)\beta_l\Gamma\left(\alpha_l+2\right)\gamma_{\alpha_l+2}\left(\frac{Th}{\beta_l}\right) + \\ \frac{c_3^l}{2}\left(\alpha_l+3\right)\beta_l\Gamma\left(\alpha_l+3\right)\gamma_{\alpha_l+3}\left(\frac{Th}{\beta_l}\right) - \\ \frac{c_3^l}{6}\beta_l\Gamma\left(\alpha_l+4\right)\gamma_{\alpha_l+4}\left(\frac{Th}{\beta_l}\right) \end{array} \tag{20}$$

In the above equation c_0^l, c_3^l, α_l and β_l are computed in (17) and (18) in terms of the first, second and third order moments m_1^l, m_2^l and m_3^l for transmitting bit "1." The function $\Gamma(\alpha_l)$ is the Gamma function which is defined as $\Gamma(\alpha_l) \triangleq \int_0^{+\infty} e^{-x}x^{\alpha_l-1}dx$. The function $\gamma_{\alpha_l}(x)$ is the incomplete Gamma function, i.e., $\gamma_{\alpha_l}(x) \triangleq \frac{1}{\Gamma(\alpha_l)}\int_0^x e^{-\tau}\tau^{\alpha_l-1}d\tau$. The integration in (19) due to the error probability PE_0^l is obtained in a closed form expression as in equation (20) except that the coefficients c_0^l, c_3^l, α_l and β_l are computed for transmitting bit "0" instead of bit "1."

C. Derivation of System Total Error Probability

The total error probability, denoted by *PE*, is obtained by averaging the conditional error probability PE_l over l as follows,

$$PE = \sum_{l=0}^{N-1} prob\left(l\right) PE_l \tag{21}$$

It should be noted that the number of active interfering users l is a random variable with binomial distribution [12]. As observed in Fig. 1, the bit interval is divided into *K* time slots and the ultrashort light pulse is in the first time slot of the bit interval. After encoding process the pulse spreads in that time slot. So the probability of one interference appearing in a time instant is obtained as $\frac{1}{2K}$. There exist $N-1$ total interfering users. Therefore, the number of active interfering users is a binomial random variable with parameters $\left(N-1, \frac{1}{2K}\right)$. Let $prob\left(l\right)$ denote the cumulative distribution function (cdf) of the number of active interfering users. So it can be obtained as follows,

$$prob\left(l\right) = \left(\begin{array}{c} N-1 \\ l \end{array}\right)\left(\frac{1}{2K}\right)^l\left(1-\frac{1}{2K}\right)^{N-1-l} \tag{22}$$

Fig. 2 compares the results of the analytic approach to evaluate the performance of SPE-OCDMA with *Thin* SHG receiver with the results of Monte-Carlo simulation. In this comparison there exist 12 active users in which a set of 12 random codes with length 511 acts as the signature sequences. Let's define $PRD \triangleq T_P/T_c$ as the ratio between the photodetector response time and the ultrashort light pulse's duration, hence small *PRD* corresponds to fast photodetectors and large *PRD* corresponds to slow photodetectors. In data recovery subsystem of the receiver *Thin* SHG crystal is employed prior to a photodetector with *PRD=25*. In each trial of Monte-Carlo simulation, the samples of a Gaussian random process due to MAI and ASE noise are generated in one bit interval

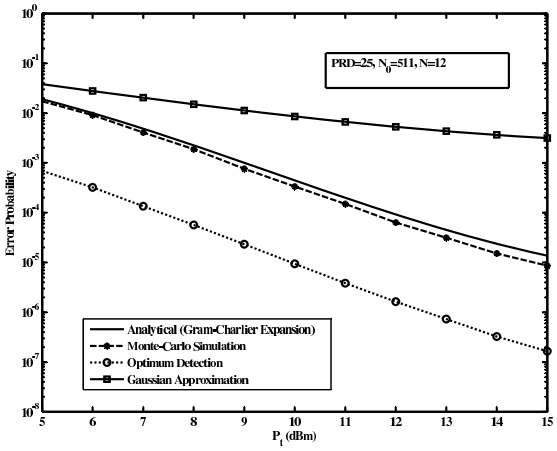

Fig. 2. Analytical and Monte-Carlo simulation performance comparison in a SPE-OCDMA system with *Thin* SHG crystal as its pre-processor (PRD=25).

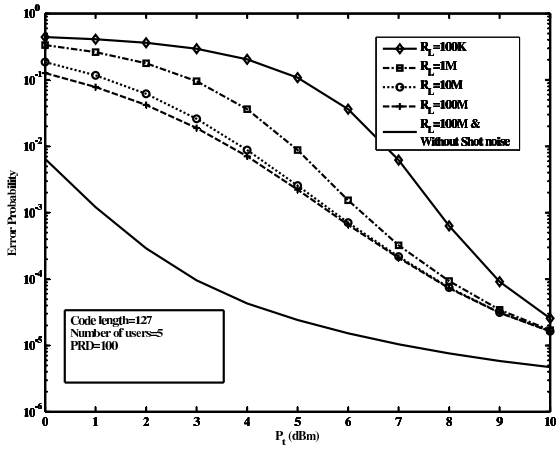

Fig. 3. Impact of the thermal noise and shot noise in the performance of *Thin* crystal receiver structure.

and are added to the samples of ultrashort light pulse. The minimum sampling time of the simulation is assumed to be $T_c/10$ which is obtained by trial and error. The summation enters into the data recovery sub-system which includes *Thin* SHG crystal followed by the photodetector. In each transmitted power level the number of trials is chosen 10 times the inverse of error probability. This figure verifies that using the Gram-Charlier expansion up to third order terms to approximate pdf of decision variable Y^l results in a good approximation in obtaining the error probability of the data recovery sub-system based on *Thin* SHG crystal. The typical values of the other parameters used for performance evaluation in Fig. 2 are shown in Table I. Fig. 2 also compares the performance of the system with the optimum detection scheme as a benchmark. In such scheme the detection process is based on comparing the sample of the decoded signal at the peak value time instant with an optimum threshold. It should be noted that the ASE noise of the optical amplifier is also considered in sketching Fig. 2.

V. Shot Noise and Thermal Noise Effect

In previous section we obtained the performance of a SPE-OCDMA with SHG crystal without including the shot noise due to the photodetector and the thermal noise due to the electronic front end stage of the receiver. To consider the above effects we redefine the decision variable at the sampler output as follows,

$$\begin{aligned} I^l &= i^l_{MAI,\,ASE,\,sh}\left(t\right) + i_{th}\left(t\right)\Big|_{@t=K_tT_b+T/2} \\ &= \tfrac{\eta q}{h\upsilon} Y^l + I_{sh} + I_{th} \end{aligned} \tag{23}$$

Where η, q, h and ν are photodetector quantum efficiency, electon charge, Plank constant and the optical frequency, respectively. In the above equation, $i^l_{MAI,\,ASE,\,sh}\left(t\right)$ indicates the flow of photoelectrons corresponding to MAI, ASE and their corresponding shot noise effects. $i_{th}\left(t\right)$ indicates the photoelectrons current due to the front end thermal noise which has a Gaussian distribution. The shot noise current conditioned on MAI and ASE is assumed to be Gaussian. Hence, conditioning on MAI and ASE, the decision variable I^l has a Gaussian distribution. Therefore the pdf of the decision variable I^l can be obtained by the convolution of the pdf due to MAI and ASE, which is obtained in the previous sections, with the pdf of the conditional shot noise and thermal noise which is Gaussian. Therefore, the pdf of the decision variable by considering thermal and shot noises is obtained as follows,

$$\begin{aligned} &Thin\,SHG,\ decision\,variable\,pdf: \\ &f_{I^l}\left(x\right) = g\left(x;0,\sigma^2_{sh,l}+\sigma^2_{th}\right) * \left(\tfrac{q\eta}{h\upsilon}\right)^{-1} f^l\left(x/\left(\tfrac{q\eta}{h\upsilon}\right)\right) \\ &Thick\,SHG,\ decision\,variable\,MGF: \\ &\Psi_{I^l}\left(s\right) = \exp\left(\tfrac{\sigma^2_{sh,l}+\sigma^2_{th}}{2}s^2\right)\Psi^l\left(s\left(\tfrac{q\eta}{h\upsilon}\right)\right) \end{aligned} \tag{24}$$

Where, $g\left(x;m,\sigma^2\right)$ denotes the Gaussian pdf with mean m and variance σ^2. $\Psi^l\left(s\right)$ and $f^l\left(x\right)$ denote the MGF and the pdf of the decision variable Y^l obtained in the previous section for both *Thick* and *Thin* crystal receiver structures. In the above equation η, h and υ are photodetector quantum efficiency, plank's constant and optical frequency, respectively. σ^2_{th} is obtained as $\sigma^2_{th} = \frac{4K_BT_r}{R_LT_p}$ for a receiver front end circuitry with temperature T_r and the equivalent resistance R_L. K_B is the Boltzmann constant. $\mu_{sh,l} = E\left(i_{MAI,\,ASE,\,sh}\left(t\right)|MAI,ASE\right)|_{@t=K_tT_b+T/2} = \left(\tfrac{q\eta}{h\upsilon}\right)E\left(Y^l\right)$ indicates the mean of the shot noise when MAI and ASE are assumed to be deterministic. The variance of the shot noise $\sigma^2_{sh,l}$ for *Thin* and *Thick* receiver structures can be obtained as $\sigma^2_{sh,l} = \frac{2q\mu_{sh,l}}{T_p}$. The conditional error probabilities $\{PE_l\}_{l=0}^{N-1}$ for *Thick* crystal receiver structure are evaluated using Saddle-Point approximation using the new MGFs obtained in equation (24). For *Thin* crystal receiver structure, the conditional error probabilities are obtained using the new pdfs in equation (24).

VI. Numerical Results

The numerical results are shown in Figs. 3–8. The typical values for the parameters used in the performance evaluation are presented in Table I. Fig. 3 and Fig. 4 show the performance of the SPE-OCDMA system for different thermal noise level for *Thin* and *Thick* crystal receiver structures respectively.

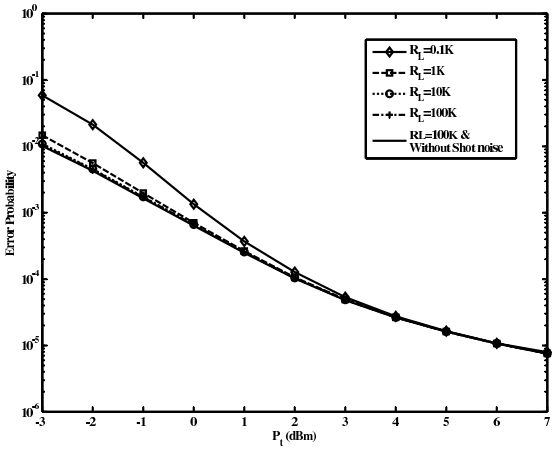

Fig. 4. Impact of the thermal noise and shot noise in the performance of *Thick* crystal receiver structure.

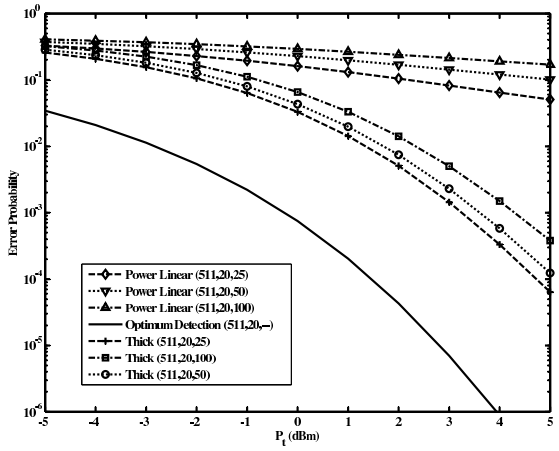

Fig. 5. Performance of power linear receiver and *Thick* crystal receiver structure for different photodetector speeds.

TABLE I
TYPICAL PARAMETER VALUES USED IN THIS PAPER

λ	Optical Wavelength	$1.55\mu m$
GVM	Group Velocity Mismatch	$0.4ps/mm$
L	Length of *Thick* crystal	$> 1cm$
P_c	The physical coefficient of the crystal	$\approx 320m^{-1}$
χ	Second order susceptibility of the crystal	$1.6 \times 10^{-8}\, esu$
κ	Dielectric constant of the crystal	4
T_c	Ultrashort pulsewidth	$400f$ sec
PRD	Processing Ratio of the Detector	25,50,100
T_r	Receiver temperature	$300^\circ K$
R_L	Load Resistance	1000Ω
G_{amp}	Gain of the optical amplifier	$30dB$
L_1	Path loss before the optical amplifier	$-10dB$
L_2	Path loss after the optical amplifier	$-5dB$
K	Excess spreading factor	5
N	Number of users	10,20
N_0	Code length	127,511

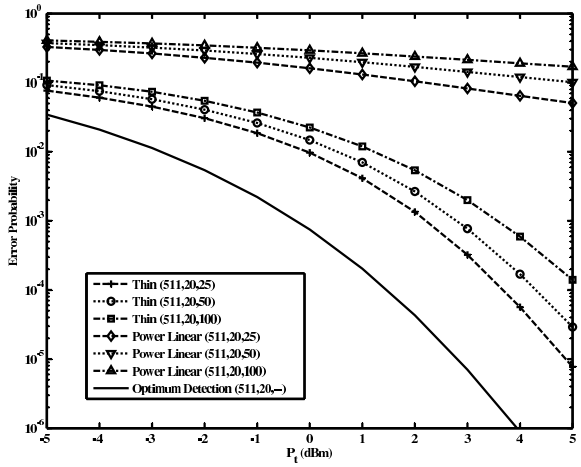

Fig. 6. Performance of power linear receiver and *Thin* crystal receiver structure for different photodetector speeds.

The impact of photodetector shot noise is also sketched in these figures. The length of signature sequence, the number of users and the PRD due to the photodetectors are fixed at 127, 5 and 100 respectively. As it is shown in Fig. 3 the performance of *Thin* crystal receiver is more sensitive to the thermal and shot noise compared to the performance of *Thick* crystal receiver. This is because of the longer length of the *Thick* crystal which provides more gain for the pulse in combating thermal and shot noises. Also, by comparing Fig. 3 and Fig. 4, we deduce that in low transmitted peak powers, e.g., less than $7dBm$, and in the presence of high level of thermal noise with $R_L = 100K\Omega$ and the shot noise, the performance of *Thick* crystal receiver structure outperforms the *Thin* crystal receiver one by several orders of magnitude.

Fig. 5 shows performance of the SPE-OCDMA system for different values of PRDs in two different conditions. In first case a simple conventional photodetector is used for the ultrashort pulse detection and in second case a nonlinear *Thick* SHG crystal is used prior to the photodetector. Fig. 6 sketches the performance of a SPE-OCDMA system with a nonlinear *Thin* crystal employed as the pre-processor, and it is compared with the performance of the receiver with a simple photodetector. As it is shown performance of the SPE-OCDMA receivers substantially degrades when the simple conventional low speed photodetector is used compare to the case in which *Thin* or *Thick* SHG crystals are employed prior to the photodetectors. The performance of the optimum detector which samples the received signal exactly at the peak value time instant is also shown as a benchmark. These figures also show that a large amount of performance improvement in the sub-optimum, but practical receivers, based on *Thin* or *Thick* SHG crystals is required.

Fig. 7 sketches the performance of *Thick* crystal receiver structure for different number of users. The transmitted peak power varies in three levels namely $P_t = -5, 0, 5dBm$ which form three curves in Fig. 7. The PRD corresponding to the photodetector is assumed to be 25 which results in 100 GHz bandwidth for a very fast photodetector impulse response when the pulse width is fixed at $400fs$. The length of the signature sequences used in the network is fixed at 127. As it is expected in each transmitted power level the performance of SPE-OCDMA receivers improves while the number of users decreases because of decreasing the variance of the MAI noise.

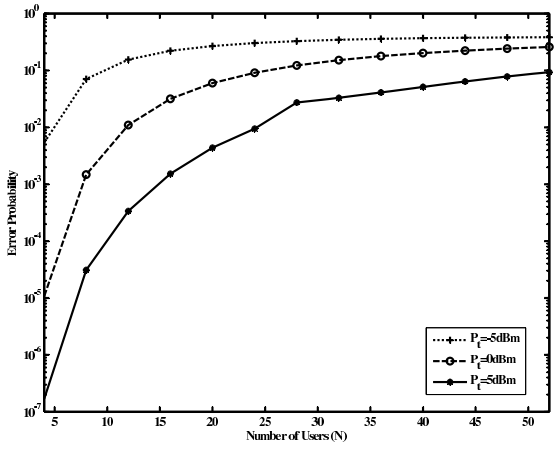

Fig. 7. Error probability versus the number of users in *Thick* crystal receiver structure.

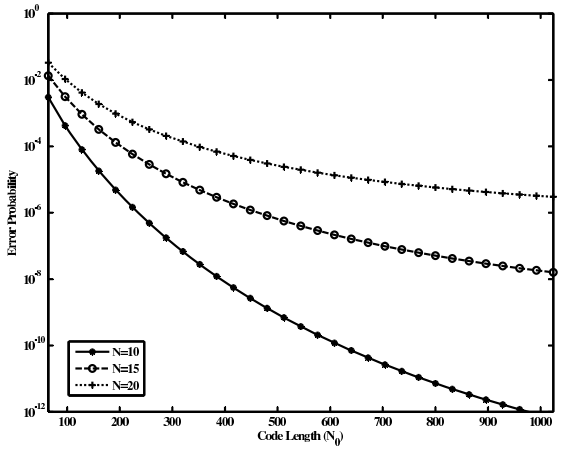

Fig. 8. Error probability versus the code length in *Thin* crystal receiver structure.

The performance degrades when the peak transmitted power decreases from $5dBm$ to $-5dBm$. The performance trend by increasing the length of signature sequence from 64 to 1024 is sketched in Fig. 8 for three cases of 10, 15 and 20 number of users. The peak power level of the transmitter is fixed at $5dBm$. The PRD due to the photodetectors used in the receiver is fixed at 25. As it is observed in this figure the performance of SPE-OCDMA receiver improves while the code length increases because of the decrease in variance due to the MAI noise.

VII. Conclusion

In this paper a nonlinear sub-system employing Second Harmonic Generation effect imposed in *Thin* and *Thick* crystals was considered as the pre-processor prior to the low-speed photodetector to overcome the difficulties in the detection of the ultrashort light pulses in a SPE-OCDMA system. We presented an in-depth analysis for the performance evaluation of the SPE-OCDMA systems with *Thin* and *Thick* crystal receiver structures. We obtained a closed form expressions as an approximation for the error probability in *Thin* crystal receiver structure and its accuracy was verified by the Monte-Carlo simulation. Using the analytical expressions the performance of SPE-OCDMA systems in terms of the code-length, the number of users and also the speed of the photodetector was presented and the amount of performance degradation due to the increase in the number of users, decrease in the code-length and decrease in photodetector speed was shown numerically. It was also shown that using the SHG crystals in the receiver the performance outperforms substantially compared to the power-linear receivers. Furthermore it was shown that even though a large amount of performance improvement is achieved by SHG crystals but their performance is still few orders of magnitudes worse than the performance of the optimum detection.

Appendix A

In this appendix the coefficients α, β, c_0 and c_3 corresponding to the pdf approximation of the decision variable *Y* in *Thin* SHG crystal data recovery sub-system is obtained. Using the Gram-Charlier expansion with the Gamma function as its kernel, the pdf $f(x)$ of the decision variable can be written as follows [18],

$$f(x) = \sum_{i=0}^{+\infty} a_i e^{-x} x^{\alpha} L_i^{\alpha}(x) \tag{A.1}$$

Where $L_i^{\alpha}(x)$ is the generalized Laguerre polynomial of degree *i* with the parameter α which is defined as follows [18],

$$L_i^{\alpha}(x) \triangleq \frac{e^{-x}x^{\alpha}}{i!}\frac{d^i}{dx^i}\left(e^{-x}x^{\alpha+i}\right) \tag{A.2}$$

The expansion coefficients $\{a_i\}_{i=0}^{\infty}$ are computed using the following orthogonality relation between the Laguerre polynomials with $\phi^{\alpha}(x) \triangleq e^{-x}x^{\alpha}$ as the weight function.

$$\begin{aligned} &\tfrac{i!}{\Gamma(\alpha+i+1)}\int_0^{\infty} e^{-x}x^{\alpha}L_i^{\alpha}(x)\,L_j^{\alpha}(x)\,dx = \delta(i,j) \\ &a_i = \tfrac{i!}{\Gamma(\alpha+i+1)}\int_0^{\infty} L_i^{\alpha}(x)\,f(x)\,dx \end{aligned} \tag{A.3}$$

Where $\delta(i,j)$ is the Kronecker delta function which is 1 when *i* and *j* are equal and otherwise it is 0. Let us define a scaling factor β and changing the expansion variable as $x \to x/\beta$ then we have [18],

$$f(x) = \sum_{i=0}^{\infty} c_i e^{-x/\beta}(x/\beta)^{\alpha} L_i^{\alpha}(x/\beta) \tag{A.4}$$

Where $\{c_i\}_{i=0}^{\infty}$ can be computed with changing the integration variable x to $t = x/\beta$ as follows,

$$c_i = \frac{i!}{\beta\Gamma(\alpha+i+1)}\int_0^{\infty} L_i^{\alpha}(x/\beta)\,f(x/\beta)\,dx \tag{A.5}$$

Because of the difficulty in obtaining higher order statistical moments used for pdf approximation, the expansion in (A.4) is computed up to fourth order. The corresponding expansion

coefficients are computed as follows [18],

$$\begin{aligned} c_0 &= \frac{m_1}{\left(m_2-m_1^2\right)\Gamma\left(\frac{m_1}{m_2-m_1^2}\right)} \\ c_1 &= \frac{1}{\beta\Gamma(\alpha+2)}\left[1+\alpha-\frac{m_1}{\beta}\right] \\ c_2 &= \frac{1}{\beta\Gamma(\alpha+3)}\left[(\alpha+1)(\alpha+2)-\frac{2m_1}{\beta}(\alpha+2)+\frac{m_2}{\beta^2}\right] \\ c_3 &= \frac{1}{\beta\Gamma(\alpha+4)}\left[\frac{m_2}{\beta^2}(\alpha+3)-\frac{m_3}{\beta^3}\right] \end{aligned} \tag{A.6}$$

In the above equation, m_1, m_2 and m_3 are the first, second and third order moments of the decision variable with pdf denoted by $f(x)$. The parameters α and β are chosen in such a way that the second and third order terms are eliminated, i.e., $c_1 = c_2 = 0$. Then we have,

$$\alpha = \frac{m_1^2}{m_2 - m_1^2} - 1 \quad , \quad \beta = \frac{m_2 - m_1^2}{m_1} \tag{A.7}$$

APPENDIX B

In this appendix we obtain closed form expressions for the first three moments of the decision variable represented in (14) for *Thin* crystal SHG crystal data recovery sub-system when bit "0" is transmitted. In this case, $r_j^l(t)$ contains only the band-limited noise $Q^l(t) = Q_x^l(t) + jQ_y^l(t)$ in which $Q_x^l(t)$ and $Q_y^l(t)$ are the quadrature components of noise. Let's define the random process $S_0^l(t)$ as $S_0^l(t) \triangleq \frac{C^2}{T_p} \times \left|r_j^l(t)\right|^4$ for transmitting bit "0," so, according to equation (14), the decision variable Y_0^l is the integral of this random process. The autocorrelation function of $S_0^l(t)$, denoted by $R_0^l(\tau)$ is evaluated using Maple software as follows,

$$R_0^l(\tau) = 64R_{Q^l}^4(\tau) + 256R_{Q^l}^2(\tau)R_{Q^l}^2(0) + 64R_{Q^l}^4(0) \tag{B.1}$$

In the above equation $R_{Q^l}(\tau)$ is the autocorrelation function of the noise $Q^l(t)$. Using the sampling theorem the random process $S_0^l(t)$ can be written as follows [19],

$$S_0^l(t) = \sum_{n=-\infty}^{+\infty} S_0^l(nT_s - T_s/2)\, Sinc\left[\frac{t + T_s/2 - nT_s}{T_s}\right] \tag{B.2}$$

Where, T_s is the sampling time corresponding to the random process $S_0^l(t)$. According to (B.1) the bandwidth of the process is four times the bandwidth of the process $Q^l(t)$ which is equal to $1/T_c$, Therefore the sampling time T_s is evaluated as $T_s = T_c/4$. Substituting (B.2) in (14) and defining $g_n \triangleq \frac{1}{T_s}\int_{-T_p/2}^{T_p/2} Sinc\left(\frac{t-nT_s}{T_s}\right)dt$ the decision variable Y_0^l for transmitting bit "0" is calculated as follows,

$$Y_0^l = \frac{1}{4PRD}\sum_{n=-\infty}^{+\infty} S_0^l(nT_s - T_s/2)\, g_n \tag{B.3}$$

Fig. 9 shows the sequence $\{g_n\}_{n=-\infty}^{+\infty}$ versus its index for a typical value of *PRD* that is equal to 100. As it is shown in this figure the sequence $\{g_n\}_{n=-\infty}^{+\infty}$ is approximated with a binary sequence. It is equal to 1 for the indices in the range of $[-2PRD, 2PRD]$ and it is equal to 0 for the other indices.Therefore, (B.3) simplifies to the following equation,

$$Y_0^l = \frac{1}{4PRD}\sum_{n=-(2PRD-1)}^{2PRD} S_0^l(nT_s - T_s/2) \tag{B.4}$$

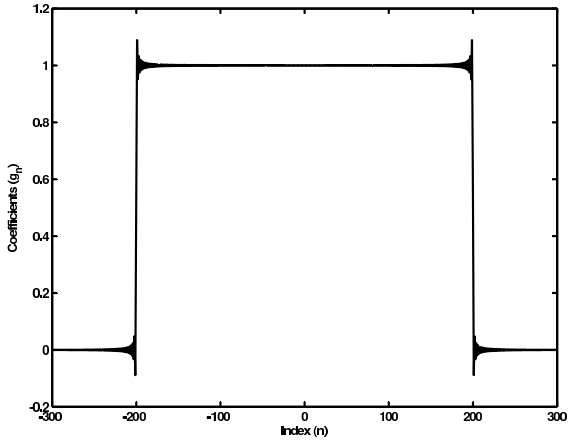

Fig. 9. The linear combination coefficients due to the decision variable in *Thin* SHG pre-processor (PRD=100).

For the sake of mathematical simplicity, let's approximate the autocorrelation function $R_{Q^l}(\tau)$ of the noise signal $Q^l(t)$ with a triangular function as follows,

$$R_{Q^l}(\tau) \approx \begin{cases} \sigma_l^2\left(1 - \frac{|\tau|}{T_c}\right) & |\tau| < T_c \\ 0 & Otherwise \end{cases} \tag{B.5}$$

In Appendix (D), the first, second and third order moments of the random variables in the form of equation (B.4), denoted by the functions $M_1^l(N_s)$, $M_2^l(N_s)$ and $M_3^l(N_s)$, are evaluated as follows,

$$\begin{aligned} m_{1,0}^l &= M_1^l(N_s) \triangleq E\left[Y_0^l\right] = 2\sigma_l^4 \times C^2 \\ m_{2,0}^l &= M_2^l(N_s) \triangleq E\left[\left(Y_0^l\right)^2\right] = \tfrac{1}{16}\tfrac{\sigma_l^8\left(814N_s - 689 + 64N_s^2\right)}{N_s^2} \times C^4 \\ m_{3,0}^l &= M_3^l(N_s) \triangleq E\left[\left(Y_0^l\right)^3\right] = \\ &= \tfrac{1}{64}\tfrac{\sigma_l^{12}\left(2.3407\times10^5 N_s + 19536N_s^2 - 3.68628\times10^5 + 512N_s^3\right)}{N_s^3} \times C^6 \end{aligned} \tag{B.6}$$

Where, N_s denotes the number of elements of the summation in (B.4), i.e., $N_s = 4PRD$.

APPENDIX C

In this appendix we obtain the closed form expressions for the first three moments of the decision variable corresponding to the *Thin* crystal SHG data recovery sub-system when bit "1" is transmitted. In this case, $r_j^l(t)$ contains both the rectangular short pulse $A(t)$ and the band-limited noise signal $Q^l(t)$. The pulse $A(t)$ is assumed to be the rectangular pulse with duration T_c and amplitude $\sqrt{P_r}$ in which P_r denotes the received peak power. So, we have,

$$A(t) = \begin{cases} \sqrt{P_r} & |t| < T_c/2 \\ 0 & Otherwise \end{cases} \tag{C.1}$$

Let's define the random process $S_1^l(t)$ as $S_1^l(t) \triangleq \frac{C^2}{T_p} \times \left|r_j^l(t)\right|^4$ when bit "1" is transmitted. The random process $S_1^l(t)$ in the interval $[-T_p/2, T_p/2]$ is studied in three sub-intervals, $I_1 = [-T_p/2, -T_c/2]$, $I_2 = [-T_c/2, T_c/2]$ and

$I_3 = [T_c/2, T_p/2]$ separately. So, the random process $S_1^l(t)$ can be written as follows,

$$S_1(t) = C^2 \times \begin{cases} \left[\left(Q_x^l(t)\right)^2 + \left(Q_y^l(t)\right)^2\right]^2 & t \in I_1 = \left[-\frac{T_p}{2}, -\frac{T_c}{2}\right] \\ \left[\begin{array}{l}\left(Q_x^l(t) + \sqrt{P_r}\right)^2 + \\ \left(Q_y^l(t)\right)^2\end{array}\right]^2 & t \in I_2 = \left[-\frac{T_c}{2}, \frac{T_c}{2}\right] \\ \left[\left(Q_x^l(t)\right)^2 + \left(Q_y^l(t)\right)^2\right]^2 & t \in I_3 = \left[\frac{T_c}{2}, \frac{T_p}{2}\right] \end{cases} \tag{C.2}$$

Therefore, the decision variable for transmitting bit "1" can be written as the summation of $N_1 = 2 \times PRD - 2$ samples of $S_0^l(t)$ in the interval I_1 and $N_2 = 4$ samples of $S_1^l(t)$ and $N_3 = 2 \times PRD - 2$ samples of $S_0^l(t)$.

$$\begin{array}{l} Y_1^l = Y^- + Y^0 + Y^+ \quad : \\ Y^- = \left[\frac{2\times PRD-2}{4\times PRD}\right] \frac{1}{2\times PRD-2} \times \\ \qquad \sum_{n=-(2\times PRD-1)}^{-2} S_1^l(nT_s - T_s/2) \\ Y^0 = \left[\frac{1}{4\times PRD}\right] \times \left[\begin{array}{l} u_1 S_1^l(-3T_s/2) + u_2 S_1^l(-T_s/2) + \\ u_3 S_1^l(T_s/2) + u_4 S_1^l(3T_s/2) \end{array}\right] \\ : \; u_j = \frac{1}{T_s} \int_{-2T_s}^{2T_s} Sinc\left(\frac{t+T_s/2-(j-2)T_s}{T_s}\right) dt \;\; , \;\; j = 1,2,3,4 \\ Y^+ = \left[\frac{2\times PRD-2}{4\times PRD}\right] \frac{1}{2\times PRD-2} \sum_{n=3}^{2\times PRD} S_1^l(nT_s - T_s/2) \end{array} \tag{C.3}$$

Where Y^-, Y^0 and Y^+ are the integral of $S_1^l(t)$ in the intervals I_1, I_2 and I_3 respectively. It is obvious that the random variables Y^- and Y^+ are independent and for mathematical simplicity the covariance between the random variables Y^0, Y^- and Y^+ is neglected. So, the first, second and third order moments of the decision variable for transmitting bit "1" are evaluated as follows,

$$\begin{array}{l} E\left[Y_1^l\right] = m_1^+ + m_1^0 + m_1^- \\ E\left[\left(Y_1^l\right)^2\right] = m_2^+ + m_2^0 + m_2^- + 2m_1^+ m_1^0 + \\ \qquad 2m_1^0 m_1^- + 2m_1^+ m_1^- \\ E\left[\left(Y_1^l\right)^3\right] = m_3^+ + m_3^0 + m_3^- + 3m_2^+ m_1^- + \\ \qquad 3m_1^+ m_2^- + 3m_1^0\left(m_2^+ + m_2^-\right) + \\ \qquad 3m_2^0\left(m_1^+ + m_1^-\right) + 6m_1^0 m_1^+ m_1^- \end{array} \tag{C.4}$$

Where, $\left\{m_1^-, m_2^-, m_3^-\right\}$, $\left\{m_1^0, m_2^0, m_3^0\right\}$ and $\left\{m_1^+, m_2^+, m_3^+\right\}$ are the corresponding moments of the random variables Y^-, Y^0 and Y^+ respectively. The moments due to the variables Y^- and Y^+ can be evaluated using the expressions related to the moments of the decision variable for transmitting bit "0." The following expressions show the relations between the moments of Y^- and Y^+ with the functions $M_1^l(N)$, $M_2^l(N)$ and $M_3^l(N)$ defined in (B.6).

$$\begin{array}{l} m_1^+ = m_1^- = \left(\frac{PRD-1}{2\times PRD}\right) M_1^l(2\times PRD - 2) \\ m_2^+ = m_2^- = \left(\frac{PRD-1}{2\times PRD}\right)^2 M_2^l(2\times PRD - 2) \\ m_3^+ = m_3^- = \left(\frac{PRD-1}{2\times PRD}\right)^3 M_3^l(2\times PRD - 2) \end{array} \tag{C.5}$$

Using the expressions for the first, second and third order moments of the normalized random variable Y_n^0 obtained in Appendix (E) the corresponding moments due to the random variable Y^0 are evaluated as follows,

$$\begin{array}{l} m_1^0 = \frac{(u_1+u_2+u_3+u_4)\left(a_0^4+8a_0^2+8\right)}{4\times PRD} \frac{\sigma_l^4}{4} \times C^2 \\ m_2^0 = \frac{\left[\begin{array}{l}\left(u_1^2+u_2^2+u_3^2+u_4^2\right)\nu_0 + \\ 2\left(u_1u_2+u_2u_3+u_3u_4\right)\nu_1 + \\ 2\left(u_1u_3+u_2u_4\right)\nu_2 + 2u_1u_4\nu_3\end{array}\right]}{(4\times PRD)^2} \frac{\sigma_l^8}{16} \times C^4 \\ m_3^0 = \frac{\left[\begin{array}{l}\left(u_1^3+u_2^3+u_3^3+u_4^3\right)\mu_{00} + \\ 6\left(u_1u_2u_3+u_2u_3u_4\right)\mu_{11} + \\ 6\left(u_1u_2u_4+u_1u_3u_4\right)\mu_{12} + \\ 3\left(\begin{array}{l} u_1^2u_2+u_1u_2^2+u_2^2u_3+u_2u_3^2 + \\ u_3^2u_4+u_3u_4^2 \end{array}\right)\mu_{10} + \\ 3\left(u_1^2u_3+u_1u_3^2+u_2^2u_4+u_2u_4^2\right)\mu_{20} + \\ 3\left(u_1^2u_4+u_1u_4^2\right)\mu_{30}\end{array}\right]}{(4\times PRD)^3} \frac{\sigma_l^{12}}{64} \times C^6 \end{array} \tag{C.6}$$

Where, $\{\nu_0, \nu_1, \nu_2, \nu_3\}$ and $\{\mu_{00}, \mu_{11}, \mu_{12}, \mu_{10}, \mu_{20}, \mu_{30}\}$ are the polynomials in $a_0 \triangleq \frac{\sqrt{P_r}}{\sqrt{\sigma_l^2/2}}$ of degree 8 and 12, respectively. The coefficients of these polynomials are computed in Appendix (E). It should be noted that Y^0 is related to Y_n^0 as $Y^0 = \frac{C^2\times\sigma_l^4/4}{4PRD} Y_n^0$.

APPENDIX D

In this appendix we obtain a closed form expression for the first, second and third order moments of the random variable $Y = \frac{1}{N_s}\sum_{m=1}^{N_s}\left(p_m^2 + q_m^2\right)^2$ in which $\vec{P} = [p_1, p_2, ..., p_{N_s}]^t$ and $\vec{Q} = [q_1, q_2, ..., q_{N_s}]^t$ are the independent zero mean Gaussian random vectors with the covariance matrix denoted by $\Theta_{N\times N}$. The (m,n)th element of the covariance matrix $\Theta_{N\times N}$ is indicated by $\theta_{m,n}$. We assume that the covariance matrix $\Theta_{N\times N}$ is a quad-diagonal matrix, i.e., all the elements of the matrix except the main diagonal and three upper and lower diagonals are equal to 0. Also it is assumed that the elements of the matrix are defined as follows,

$$\theta_{m,n} = \frac{\sigma_l^2}{2}\begin{cases} 1 - \frac{|m-n|}{4} & |m-n| < 4 \\ 0 & Otherwise \end{cases} \tag{D.1}$$

Let us define the random variables $X_i \triangleq \left(p_i^2 + q_i^2\right)^2$, $i = 1, 2, ..., N$.

A. First Order Moment:

The statistics of the pair $\{p_i, q_i\}$ is unchanged by varying the index *i*. So, the first moment of the random variable *Y* is computed as follows,

$$\begin{array}{l} M_1^l(N_s) \triangleq E\left[\frac{1}{N_s}\sum_{n=1}^{N_s} X_i\right] = \frac{1}{N_s}\sum_{n=1}^{N_s} E[X_i] \\ \qquad = E[X_1] = 2\sigma_l^4 \times C^2 \end{array} \tag{D.2}$$

B. Second Order Moment:

The expected value due to the square of the random variable *Y* is computed as follows,

$$\begin{array}{l} M_1^l(N_s) \triangleq E\left[\frac{1}{N_s}\sum_{n=1}^{N_s} X_i\right] = \frac{1}{N_s}\sum_{n=1}^{N_s} E[X_i] \\ \qquad = E[X_1] = 2\sigma_l^4 \times C^2 \end{array} \tag{D.3}$$

We can classify the terms in the summation (D.3) into five distinct classes such that the elements in each class have the same values in that summation. In fact $E[X_iX_j]$ belongs

TABLE II
THE NUMBER OF ELEMENTS AND THE CORRESPONDING VALUES OF THE CLASSES FOR SECOND ORDER MOMENT

Class Number	Number of elements	The corresponding value
1	$num_0 = N_s$	$s_0 = 384\left(\sigma_l^8/16\right) \times C^4$
2	$num_1 = 2\left(N_s - 1\right)$	$s_1 = (228.25)\left(\sigma_l^8/16\right) \times C^4$
3	$num_2 = 2\left(N_s - 2\right)$	$s_2 = 132\left(\sigma_l^8/16\right) \times C^4$
4	$num_3 = 2\left(N_s - 3\right)$	$s_3 = 78.75\left(\sigma_l^8/16\right) \times C^4$
5	$num_4 = N_s^2 - 7N_s - 12$	$s_4 = 4\sigma_l^8 \times C^4$

to class1 when $|i-j|$, belongs to class2 when $|i-j|=0$, belongs to class3 when $|i-j|=1$, belongs to class4 when $|i-j|=2$ and finally it belongs to class5 when $|i-j| \geq 4$. The number of elements in each class and its corresponding value is evaluated using the Maple software and are represented in Table II. By substituting the values of each class in the summation (D.3) and doing some algebra, the second order moment of the random variable Y is obtained as follows,

$$M_2^l\left(N_s\right) = \frac{1}{N_s^2}\left(\begin{array}{l} num_0 s_0 + num_1 s_1 + \\ +num_2 s_2 + num_3 s_3 + num_4 s_4 \end{array}\right) = \\ = \frac{1}{16}\frac{\sigma_l^8\left(814N_s - 689 + 64N_s^2\right)}{N_s^2} \times C^4 \tag{D.4}$$

C. Third Order Moment:

The expected value due to the cube of the random variable Y is computed as follows,

$$M_3^l\left(N\right) \triangleq E\left[\left(\frac{1}{N_s}\sum_{n=1}^{N_s} X_i\right)^3\right] \\ = \frac{1}{N_s^3}\sum_{i=1}^{N_s}\sum_{j=1}^{N_s}\sum_{k=1}^{N_s} E\left(X_i X_j X_k\right) \tag{D.5}$$

To obtain a closed expression for the above summation, the terms are classified into 15 different classes in such a way that the elements in each class have the same value. In fact, $E\left(X_i X_j X_k\right)$ belongs to class1 when ($|i-j|=0$, $|j-k|=0$), belongs to class2 when ($|i-j|=1$, $|j-k|=0$), belongs to class3 when ($|i-j|=2$, $|j-k|=0$), belongs to class4 when ($|i-j|=3$, $|j-k|=0$), belongs to class5 when ($|i-j|=1$, $|j-k|=1$), belongs to class6 when ($|i-j|=1$, $|j-k|=2$), belongs to class7 when ($|i-j|=1$, $|j-k|=3$), belongs to class8 when ($|i-j|=2$, $|j-k|=2$), belongs to class9 when ($|i-j|=2$, $|j-k|=3$), belongs to class10 when ($|i-j|=3$, $|j-k|=3$), belongs to class11 when ($|i-j|=0$, $|j-k| \geq 4$), belongs to class12 when ($|i-j|=1$, $|j-k| \geq 4$), belongs to class13 when ($|i-j|=2$, $|j-k| \geq 4$), belongs to class14 when ($|i-j|=3$, $|j-k| \geq 4$) and finally it belongs to class15 when ($|i-j| \geq 4$, $|j-k| \geq 4$). The number of elements in each class and also their corresponding values, computed in Maple software, are shown in Table III. By substituting the values of each class in the summation (D.5) and doing some algebra, the third order moment of the random variable Y is obtained as follows,

TABLE III
THE NUMBER OF ELEMENTS AND THE CORRESPONDING VALUES OF THE CLASSES FOR THIRD ORDER MOMENT

Class Number	Number of elements	The corresponding value
1	$num_0 = N_s$	$m_{0,0} = E\left(X_1^3\right) = 46080\left(\sigma_l^{12}/64\right) \times C^6$
2	$num_1 = 6N_s - 6$	$m_{0,1} = E\left(X_1 X_2^2\right) = 22182\left(\sigma_l^{12}/64\right) \times C^6$
3	$num_2 = 6N_s - 12$	$m_{0,2} = E\left(X_1 X_3^2\right) = 10368\left(\sigma_l^{12}/64\right) \times C^6$
4	$num_3 = 6N_s - 18$	$m_{0,3} = E\left(X_1 X_4^2\right) = 4680\left(\sigma_l^{12}/64\right) \times C^6$
5	$num_4 = 6N_s - 12$	$m_{1,1} = E\left(X_1 X_2 X_3\right) = 10425\left(\sigma_l^{12}/64\right) \times C^6$
6	$num_5 = 12N_s - 36$	$m_{1,2} = E\left(X_1 X_2 X_4\right) = 4433\left(\sigma_l^{12}/64\right) \times C^6$
7	$num_6 = 12N_s - 48$	$m_{1,3} = E\left(X_1 X_2 X_5\right) = 2100\left(\sigma_l^{12}/64\right) \times C^6$
8	$num_7 = 6N_s - 24$	$m_{2,2} = E\left(X_1 X_3 X_5\right) = 1856\left(\sigma_l^{12}/64\right) \times C^6$
9	$num_8 = 12N_s - 60$	$m_{2,3} = E\left(X_1 X_3 X_6\right) = 1250\left(\sigma_l^{12}/64\right) \times C^6$
10	$num_9 = 6N_s - 36$	$m_{3,3} = E\left(X_1 X_4 X_7\right) = 788\left(\sigma_l^{12}/64\right) \times C^6$
11	$num_{10} = 3N_s^2 - 21N_s + 36$	$m_{0,x} = E\left(X_1^2\right) E\left(X_1\right) = 3072\left(\sigma_l^{12}/64\right) \times C^6$
12	$num_{11} = 6N_s^2 - 54N_s + 120$	$m_{1,x} = E\left(X_1 X_2\right) E\left(X_1\right) = 1826\left(\sigma_l^{12}/64\right) \times C^6$
13	$num_{12} = 6N_s^2 - 66N_s + 180$	$m_{2,x} = E\left(X_1 X_3\right) E\left(X_1\right) = 1056\left(\sigma_l^{12}/64\right) \times C^6$
14	$num_{13} = 6N_s^2 - 78N_s + 252$	$m_{3,x} = E\left(X_1 X_4\right) E\left(X_1\right) = 630\left(\sigma_l^{12}/64\right) \times C^6$
15	$num_{14} = N_s^3 - 21N_s^2 + 146N_s - 336$	$m_{x,x} = E^3\left(X_1\right) = 512\left(\sigma_l^{12}/64\right) \times C^6$

$$M_3^l\left(N\right) = \\ \frac{1}{N_s^3}\left(\begin{array}{l} num_0 m_{0,0} + num_1 m_{1,0} + num_2 m_{2,0} \\ +num_3 m_{3,0} + num_4 m_{1,1} + num_5 m_{1,2} \\ +num_6 m_{1,3} + num_7 m_{2,2} + num_8 m_{2,3} \\ +num_9 m_{3,3} + num_{10} m_{0,x} + num_{11} m_{1,x} \\ +num_{12} m_{2,x} + num_{13} m_{3,x} + num_{14} m_{x,x} \end{array}\right) = \\ = \frac{1}{64}\frac{\sigma_l^{12}\left(\begin{array}{l} 2.3407 \times 10^5 N_s + 19536N_s^2 \\ -3.68628 \times 10^5 + 512N_s^3 \end{array}\right)}{N_s^3} \times C^6 \tag{D.6}$$

APPENDIX E

In this appendix we obtain the first, second and third order moments of the normalized random variable $Y_n^0 = u_1 X_1 + u_2 X_2 + u_3 X_3 + u_4 X_4$. In this expression the random variables $\{X_i\}_{i=1}^4$ are defined as $X_i \triangleq \left(P_i^2 + q_i^2\right)^2$, $i = 1,2,3,4$ where the random vectors $\vec{P} = [P_1, P_2, P_3, P_4]^t$ and $\vec{Q} = [q_1, q_2, q_3, q_4]^t$ are independent Gaussian vectors. $\vec{Q}$ is a zero mean random vector and $[a_0, a_0, a_0, a_0]^t$ is the mean value corresponding to the random vector $\vec{P}$ where a_0 is defined as $a_0 \triangleq \frac{\sqrt{P_r}}{\sqrt{\sigma_l^2/2}}$. The covariance matrix due to these vectors are denoted by $\Theta_{4\times4}$ that is defined as follows,

$$\Theta_{4\times4} = \begin{bmatrix} 1.00 & 0.75 & 0.50 & 0.25 \\ 0.75 & 1.00 & 0.75 & 0.50 \\ 0.50 & 0.75 & 1.00 & 0.75 \\ 0.25 & 0.50 & 0.75 & 1.00 \end{bmatrix} \tag{E.1}$$

By squaring and cubing the random variable Y_n^0 and doing some simple algebra we have,

$$\begin{aligned}
m_{0,1} &= E\left(Y_n^0\right) = \left(u_1+u_2+u_3+u_4\right)E\left(X_1\right)\\
m_{0,2} &= E\left[\left(Y_n^0\right)^2\right] = \left(u_1^2+u_2^2+u_3^2+u_4^2\right)E\left(X_1^2\right)+\\
&\quad 2\left(u_1u_2+u_2u_3+u_3u_4\right)E\left(X_1X_2\right)+\\
&\quad 2\left(u_1u_3+u_2u_4\right)E\left(X_1X_3\right)+2u_1u_4E\left(X_1X_4\right)\\
m_{0,3} &= E\left[\left(Y_n^0\right)^3\right] = \left(u_1^3+u_2^3+u_3^3+u_4^3\right)E\left(X_1^3\right)+\\
&\quad 6\left(u_1u_2u_3+u_2u_3u_4\right)E\left(X_1X_2X_3\right)+\\
&\quad 6\left(u_1u_2u_4+u_1u_3u_4\right)E\left(X_1X_2X_4\right)+\\
&\quad 3\left(u_1^2u_3+u_1u_3^2+u_2^2u_4+u_2u_4^2\right)E\left(X_1^2X_3\right)+\\
&\quad 3\left(\begin{array}{c}u_1^2u_2+u_1u_2^2+u_2^2u_3+\\ u_2u_3^2+u_3^2u_4+u_3u_4^2\end{array}\right)E\left(X_1^2X_2\right)+\\
&\quad 3\left(u_1^2u_4+u_1u_4^2\right)E\left(X_1^2X_4\right)
\end{aligned} \tag{E.2}$$

The terms related to the correlations among the elements of the set $\{X_i\}_{i=1}^4$ is obtained using the Maple software and can be represented by the polynomials of the input pulse amplitude a_0 as the following expressions.

$$\begin{aligned}
&E\left(X_1\right) = a_0^4+8a_0^2+8\\
&\nu_0 \triangleq E\left(X_1^2\right) = a_0^8+32a_0^6+288a_0^4+768a_0^2+384\\
&\nu_1 \triangleq E\left(X_1X_2\right) = a_0^8+28a_0^6+221a_0^4+518a_0^2+228.25\\
&\nu_2 \triangleq E\left(X_1X_3\right) = a_0^8+24a_0^6+164a_0^4+336a_0^2+132\\
&\nu_3 \triangleq E\left(X_1X_4\right) = a_0^8+20a_0^6+117a_0^4+208.5a_0^2+78.75\\
&\mu_{00} \triangleq E\left(X_1^3\right) = a_0^{12}+72a_0^{10}+1800a_0^8+19200a_0^6+\\
&\qquad 86400a_0^4+138240a_0^2+46080\\
&\mu_{10} \triangleq E\left(X_1^2X_2\right) = a_0^{12}+64a_0^{10}+1422a_0^8+13441a_0^6+\\
&\qquad 53328a_0^4+74925a_0^2+22182\\
&\mu_{20} \triangleq E\left(X_1^2X_3\right) = a_0^{12}+56a_0^{10}+1088a_0^8+9024a_0^6+\\
&\qquad 31632a_0^4+39552a_0^2+10368\\
&\mu_{30} \triangleq E\left(X_1^2X_4\right) = a_0^{12}+48a_0^{10}+798a_0^8+5688a_0^6+\\
&\qquad 17289a_0^4+19080a_0^2+4680\\
&\mu_{11} \triangleq E\left(X_1X_2X_3\right) = a_0^{12}+56a_0^{10}+1090a_0^8+9064a_0^6+\\
&\qquad 31849a_0^4+36870a_0^2+10425\\
&\mu_{12} \triangleq E\left(X_1X_2X_4\right) = a_0^{12}+48a_0^{10}+802a_0^8+5744a_0^6+\\
&\qquad 17473a_0^4+1909a_0^2+4433
\end{aligned} \tag{E.3}$$

The polynomials are of degree 8 and 12 for computing the second order moment $m_{0,2}$ and the third order moment $m_{0,3}$ respectively. Therefore, by substituting the above values in (E.2) the first, second and third order moments corresponding to the random variable Y is obtained as follows,

$$\begin{aligned}
&m_{0,1} = E\left(Y_n^0\right) = \left(u_1+u_2+u_3+u_4\right)\left(a_0^4+8a_0^2+8\right)\\
&m_{0,2} = E\left[\left(Y_n^0\right)^2\right] = \left(u_1^2+u_2^2+u_3^2+u_4^2\right)\nu_0+\\
&2\left(u_1u_2+u_2u_3+u_3u_4\right)\nu_1+2\left(u_1u_3+u_2u_4\right)\nu_2+2u_1u_4\nu_3\\
&m_{0,3} = E\left[\left(Y_n^0\right)^3\right] = \left(u_1^3+u_2^3+u_3^3+u_4^3\right)\mu_{00}+\\
&6\left(u_1u_2u_3+u_2u_3u_4\right)\mu_{11}+6\left(u_1u_2u_4+u_1u_3u_4\right)\mu_{12}+\\
&3\left(u_1^2u_3+u_1u_3^2+u_2^2u_4+u_2u_4^2\right)\mu_{02}+\\
&3\left(u_1^2u_2+u_1u_2^2+u_2^2u_3+u_2u_3^2+u_3^2u_4+u_3u_4^2\right)\mu_{01}+\\
&3\left(u_1^2u_4+u_1u_4^2\right)\mu_{03}
\end{aligned} \tag{E.4}$$

REFERENCES

[1] J. A. Salehi, "Emerging OCDMA communication systems and data networks" (invited), *J. Optical Networking*, vol. 6, no. 9, pp. 1138–1178, Sep. 2007.

[2] Z. Jiang, D. S. Seo, S. D. Yang, D. E. Leaird, R. V. Roussev, C. Langrock, M. M. Fejer, and A. M. Weiner, "Four-user 2.5Gb/s spectrally coded OCDMA system demonstration using low power nonlinear processing," *IEEE J. Lightwave Technol.*, vol. 23, no. 1, pp. 143–158, Mar. 2005.

[3] Z. Zheng, A. M. Weiner, J. H. Marsh, and M. M. Karkhanehchi, "Ultrafast optical thresholding based on two-photon absorption GaAs waveguide photodetectors," *IEEE Photon. Technol. Lett.*, vol. 9, no. 4, pp. 493–495, Apr. 1997.

[4] R. P. Scott, W. Cong, V. J. Hernandez, K. Li, B. H. Kolner, J. P. Heritage, and S. J. Ben Yoo, "An eight-user time slotted SPECTS O-CDMA testbed: demonstration and simulations," *IEEE J. Lightwave Technol.*, vol. 24, no. 1, Jan. 2006.

[5] T. Hamanaka, X. Wang, N. Wada, A. Nishiki, and K. Kitayama, "Ten-user truly asynchronous gigabit OCDMA transmission experiment with a 511-chip SSFBG en/decoder," *IEEE J. Lightwave Technol.*, vol. 24, no. 1, Jan. 2006.

[6] J. Cao, R. G. Broeke, N. K. Fontaine, C. Ji, Y. Du, N. Chubun, K. Aihara, A. Pham, F. Olsson, S. Lourdudoss, and S. J. Ben Yoo, "Demonstration of spectral phase O-CDMA encoding and decoding in monolithically integrated arrayed-waveguide-grating-based encoder," *IEEE Photonics Technol. Lett.*, vol. 18, no. 24, Dec. 2006.

[7] K. Jamshidi and J. A. Salehi, "Statistical characterization and bit-error rate analysis of lightwave systems with optical amplification using two-photon- absorption receiver structures," *IEEE J. Lightwave Technol.*, vol. 24, no. 3, pp. 1302–1316, Mar. 2006.

[8] K. Jamshidi and J. A. Salehi, "Performance analysis of spectral-phase-encoded optical CDMA system using two-photon-absorption receiver structure for asynchronous and slot-level synchronous transmitters," *IEEE J. Lightwave Technol.*, vol. 25, no. 6, pp. 1638–1645, June 2007.

[9] B. Ni, J. S. Lehnert, and A. M. Weiner, "Performance of nonlinear receivers in asynchronous spectral-phase-encoding optical CDMA systems," *IEEE J. Lightwave Technol.*, vol. 25, no. 8, pp. 2069–2080, Aug. 2007.

[10] Y. Igarashi and H. Yashima, "Performance analysis of coherent ultrashort light pulse CDMA communication systems with nonlinear optical thresholder," *IEICE Trans. Commun.*, vol. E89B, no. 4, Apr. 2006.

[11] M. D. Matinfar and J. A. Salehi, "Mathematical modeling and statistical analysis of second harmonic generation effects with *thin* and *thick* crystals in ultrahigh speed optically amplified digital lightwave communication systems," *IEEE J. Lightwave Technol.*, vol. 27, no. 16, pp. 3438–3452, Aug. 2009.

[12] J. A. Salehi, A. M. Weiner, and J. P. Heritage, "Coherent ultrashort light pulse code-division multiple access communication systems," *IEEE J. Lightwave Technol.*, vol. 8, no. 3, Mar. 1990.

[13] P. A. Humblet and M. Azizoglu, "On the bit error rate of lightwave systems with optical amplifiers," *IEEE J. Lightwave Technol.*, vol. 9, no. 11, pp. 1576–1582, Nov. 1991.

[14] W. H. Glenn, "Second harmonic generation by picosecond optical pulses," *IEEE J. Quantom Electron.*, vol. 5, no. 6, pp. 284–290, June 1969.

[15] A. Papoulis, "Narrow-band systems and Gaussianity," *IEEE Trans. Inf. Theory*, vol. 18, no. 1, pp. 20–27, Jan. 1972.

[16] L. Turin, "The characteristic function of Hermitian quadratic forms in complex normal variables," *Biometrika*, vol. 47, nos. 1–2, June 1960.

[17] C. W. Helstrom, "Approximate evaluation of detection probabilities in radar and optical communications," *IEEE Trans. Aerosp. Electron. Syst.*, vol. 14, pp. 630–640, July 1978.

[18] J. Marcum, "A statistical theory of target detection by pulsed radar," *IRE Trans. Inf. Theory*, vol. 6, no. 2, pp. 59–260, Apr. 1960.

[19] A. Papoulis and S. U. Pillai, *Probability, Random Variables and Stochastic Processes*. McGraw Hill, 2002.

[20] R. W. Boyd, *Nonlinear Optics*, 2nd edition. Academic Press, 2003.

[21] G. P. Agrawal, *Fiber-Optic Communication Systems*, 3rd edition. John Wiley and Sons, 2002.

[22] K. Jamshidi and J. A. Salehi, "Statistical analysis of coherent ultrashort light pulse CDMA with multiple optical amplifiers using additive noise model," *J. Lightwave Technol.*, vol. 23, no. 5, pp. 1842–1851, May 2005.

Mehdi D. Matinfar (S'06) was born in Tehran, Iran, in May 1980. He received the B.S. degree from Sharif University of Technology (SUT), Tehran, in 2002, the M.S. degree from Khajeh Nasir University of Technology (KNUT), Tehran, in 2004, and the Ph.D. degree from SUT, in 2010, all in electrical engineering. From June 2001 to September 2002, he was a Member of Research Staff of the Mobile Communications Division at the Iran Telecommunication Research Center (ITRC), and since 2003, he has been with the Optical Networks Research Lab (ONRL) as a Member of Technical Staff. His research interests include ultrahigh-speed optical communications, nonlinear optical detection, wireless communication systems and optical communication systems, specifically, optical CDMA and indoor optical communications.

Jawad A. Salehi (M'84-SM'07-F10) was born in Kazemain, Iraq, on December 22, 1956. He received the B.S. degree from the University of California, Irvine, in 1979, and the M.S. and Ph.D. degrees from the University of Southern California (USC), Los Angeles, in 1980 and 1984, respectively, all in electrical engineering. He is currently a Full Professor at the Optical Networks Research Laboratory (ONRL), Department of Electrical Engineering, Sharif University of Technology (SUT), Tehran, Iran, where he is also the Co-founder of the Advanced Communications Research Institute (ACRI). From 1981 to 1984, he was a full-time Research Assistant at the Communication Science Institute, USC. From 1984 to 1993, he was a Member of Technical Staff of the Applied Research Area, Bell Communications Research (Bellcore), Morristown, NJ. During 1990, he was with the Laboratory of Information and Decision Systems, Massachusetts Institute of Technology (MIT), Cambridge, as a Visiting Research Scientist. From 1999 to 2001, he was the Head of the Mobile Communications Systems Group and the Co-director of the Advanced and Wideband Code-Division Multiple Access (CDMA) Laboratory, Iran Telecom Research Center (ITRC), Tehran. From 2003 to 2006, he was the Director of the National Center of Excellence in Communications Science, Department of Electrical Engineering, SUT.

He is the holder of 12 U.S. patents on optical CDMA. His current research interests include optical multiaccess networks, optical orthogonal codes (OOC), fiber-optic CDMA, femtosecond or ultrashort light pulse CDMA, spread-time CDMA, holographic CDMA, wireless indoor optical CDMA, all-optical synchronization, and applications of erbium-doped fiber amplifiers (EDFAs) in optical systems. Prof. Salehi is an Associate Editor for Optical CDMA of the IEEE TRANSACTIONS ON COMMUNICATIONS since May 2001. In September 2005, he was elected as the Interim Chair of the IEEE Iran Section. He was the recipient of several awards including Bellcore's Award of Excellence, the Nationwide Outstanding Research Award from the Ministry of Science, Research, and Technology in 2003, and the Nation's Highly Cited Researcher Award in 2004. In 2007, he received the Khwarazmi International Prize, first rank, in fundamental research and also the Outstanding Inventor Award (Gold medal) from the World Intellectual Property Organization (WIPO), Geneva, Switzerland. In 2010, he was promoted to IEEE fellow grade for contributions to the "fundamental principles in optical code division multiple access." He is among the 250 pre-eminent and most influential researchers worldwide in the Institute for Scientific Information (ISI), Highly Cited in the Computer-Science Category.